明新學報 44 卷 第 2 期 PP.1-17
Vol. 44, No. 2, Minghsin Journal, Dec. 2021

應用臨場氧/氬氣電漿處理銀薄膜之高品質係數氧化銦錫/銀多層透明電極

彭政雄，張博學，王政穎，陳邦旭

明新科技大學化學工程與材料科技系 地址：新竹縣新豐鄉新興路 1 號

摘要

在本研究中，使用濺射沉積將銦錫氧化物 (ITO) 膜和 Ag 膜沉積在玻璃基板上。使用 X 射線繞射法和紫外-可見光譜法鑑定使用濺射沉積法成長的銦錫氧化物的晶體結構和光學性能的特性。在室溫下濺射沉積所製備的銦錫氧化物薄膜之晶體結構呈現非晶相；計算可得其直接光學能隙為 3.62 eV。針對銦錫氧化物膜/銀膜/銦錫氧化物膜三層結構，在成長最後一層銀箔膜之前，採用臨場 O_2/Ar 電漿表面處來改變 Ag 層的表面形貌。這種方法提高了具有相同薄層電阻 (Rs) 下的 Ag/ITO 雙層的可見光穿透射率。X 射線繞射顯示，Ag 薄膜中具有沿（111）和（200）方向晶面方向的多晶晶粒。可以為上下層的銦錫氧化物薄膜提供載流子並降低 ITO/Ag 多層膜的薄膜片電阻。具有適當 Ag 厚度 (> 10 奈米) 的三層層顯示其具有低電阻和高可見光穿透率。同時研究了，Ag 和銦錫氧化物厚度對 銦錫氧化物/Ag/銦錫氧化物 (IAI) 光學和電學特性的相關性。使用品質係數(Figure of Merit)用於尋找具有最優異導電性和透明度的銦錫氧化物膜/銀膜/銦錫氧化物膜三層結構層。本研究成功的製備了用於銦錫氧化物膜/銀膜/銦錫氧化物膜三層結構層在 550 nm 波長光子下的品質係數為 1.09×10^{-1} (Ω^{-1})

關鍵字： 銦錫氧化物，銀，濺射沉積，透明電極，臨場電漿處理

High transparent ITO/Ag based electrodes with Ag midlayer under O_2/Ar plasma exposure

Cheng-Hsiung Peng, Po-Hsueh Chang, Zheng Ying Wang, Pang Shiu Chen

Department of Chemical and Materials Engineering, MingHsin University of Science and Technology, Hsinfeng, Hsinchu 304, Taiwan, ROC

Abstract

Indium-tin oxide (ITO) films and Ag films were deposited on glass by using sputtering-deposition. The details regarding crystal structure and optical properties of the ITO films were examined using X-ray diffraction and ultraviolet-visible spectrometry. The as-prepared ITO film exhibited an amorphous phase with a direct optical band gap of 3.62 eV. In-situ O_2/Ar plasma was adopted to modify surface morphology of the Ag layer. This approach enhanced the transmittance of Ag/ITO bilayers with the same sheet resistance (*R*s). The poly-grains oriented along (111) and (200) directions in the Ag thin films could supply

carriers into the ITO film and lower the *R*s of the ITO/Ag multilayer. The multilayer with an appropriate Ag thickness (> 10 nm) showed low resistance and high visible transmittance. Dependence of the Ag and ITO thickness on the optical and electrical properties of ITO/Ag/ITO (IAI) were explored. A figure of merit (FOM) was used to find an optimal layer with superior conductivity and transparency. A FOM of 1.09×10^{-1} (Ω^{-1}) at the wavelength of 550 nm for an IAI layer was prepared. Thermal stability of IAI multilayers ranging from 200 to 500 ºC were also explored. The IAI annealed at 400 ºC achieved an optimized FOM of 1.56×10^{-1} Ω^{-1}.

.

Keywords: indium tin oxide; silver; sputtering system; transparent conductive electrode; in-situ plasma

1. Introduction

Recently, indium tin oxide (ITO) layers have been demonstrated low resistivity and high transmittance in the visible range of the spectrum, and the layers are widely used as transparent conductive oxide (TCO) in solar cells, flat panel display, organic light emitting diodes, or electrochromic devices [1]. High conductivity ITO thin films have been achieved by using sputtering, the films were usually prepared by grown or annealed at high temperature > 300 oC [2]. Beside, ITO thin films also exhibit poor mechanical properties due to its brittle properties [3]. Owing to limited resource on earth, the cost of In element is expensive [4]. Hence, these characteristics will limit the applications of ITO film in low-temperature processes. However, ITO film shows high electrical stability in high temperature and high humidity environment [5].

Dielectric-metal-dielectric (DMD) sandwiched film structures with different metal mid-layers have been explored to enhance the visible transmission and near-infrared reflectance of TCOs without significantly degrading conductivity at low temperature process and ensuring the long term electrical stability [6,7]. Especially, the flexibility of DMD due to the ductile inserted metal layer is suitable for wearable devices or flexible electronics [8]. ZnO:Al, ZnO:Ga, TiO2 and MoO3 are among the most widely studied dielectric films in DMD structures. In such structures, an inserted metal layer with low conductivity is required. It is well known that Au [9], Al [10], Cu [11], Pt [12], Ni [13] and Ag [14, 15] all show good conductivity. Furthermore, Ag has been shown to exhibit the lowest absorptivity in the visible region as a thin metal layer [16]. Some research groups also adopted ITO/Ag/ITO (IAI) stacking structures to produce transparent films for organic photovoltaic (OPV), organic light emitting diode, and ultraviolet light emitting diode [17-19]. There are several advantages with IAI stacking layer structure. First, in the usage of ITO, one of the advantages is the reduction of the consumption of In by decrease ITO film thickness for both ITO layer with high electrical stability. Second, the mechanical properties can be improved due to the ductile characteristics of the Ag metal layer. Some studies have reported an improved conversion efficiency of OPV cells with an IAI structure [17]. The Ag mid-layer plays an

important role in achieving low resistivity in DMD structures with enough visible transmittance. The conductivity and transparence of a thin Ag layer should be optimized at a percolation critical thickness that is the minimum thickness for a continuous layer with sufficient electrical path. Wang et al. prepared a promising 6-nm-thick O-doped Ag electrode through reactive sputtering by introducing a gas mixture of O_2 and Ar. They proposed that the O inclusion will retard the surface migration of Ag, which leads to form a two-dimensional continuous layer with high transparence at smaller film thickness. However, the coverage of Ag layer seems sensitive on the buried layer due to its wetting property with substrate, Ag layer exhibited poor wetting behavior on ITO layer [20]. Some studies used an optimized growth rate of Ag layer with surface coverage during deposition. This can enhance the transparence of MoO3/Ag/MoO3 multilayer with a low sheet resistance (Rs) [21, 22]. Low energy plasma, consisted of partially ionized O species, was used to modify the surface morphology of Ag nanoclusters [23] and change the optical properties of Ag/Si3N4. Hence, in this work, all films were prepared by sputtering. The structure, chemical bonding, and optical properties of ITO prepared by reactive sputtering were characterized. The Ag layers after deposition were exposed under radio frequency (RF) plasma with different O2/Ar gas flow rate ratio and duration. The thickness effects of ITO or Ag for the Ag/ITO (AI), IAI stacked layers were also analyzed to tailor the transparency and electrical properties of the fabricated AI or IAI films.

2. Experimental

ITO films and embedded Ag layers were prepared on soda-lime glass in a sputtering system. ITO ceramic targets were used for the deposition of ITO and the sputtering was performed in the presence of O_2 and Ar as reactive gases. All of the glass substrates were initially cleaned with acetone and methyl alcohol and then submitted to an radio frequency (RF) oxygen-plasma treatment at 50 W for 3 min. The base pressure of the system reached 1.1×10^{-3} Pa. The targets used in this work were commercially available ITO (In_2O_3:SnO_2 = 10:1; 99.99% purity; 10 cm in diameter) and Ag (99.99% purity; 10 cm in diameter). Before the deposition of the ITO bottom layer (BL), the target was cleaned with sputtering for 10 min to remove the surface contamination. Then, the samples were coated with a 60-nm-thick ITO layer on glass at room temperature (RT) to explore the properties of the ITO layer. Using the same deposition parameters, ITO layers with different thicknesses were deposited on the soda-lime glass at RT, followed by the insertion of Ag layers with different thicknesses; finally, some of the samples were covered with ITO capping layers, before the deposition of ITO over layer (OL), the inserted Ag layers were exposed to various ration of O_2/Ar plasma with different process time. The symbols A, A(n)I, I(n)A, and IA(*n*)I denote samples with *n*-nm-thick Ag or ITO layers.

The structural properties of the multilayers were identified by applying grazing incident-angle X-ray diffraction (GIAXRD) or θ-2θ diffraction, which was performed using an X-ray diffractometer with Cu-$K\alpha_1$ radiation (λ=0.154056 nm). In addition, the crystallite size (D) of the stacked films was

calculated by the X-ray line-broadening technique performed on the (111) and (220) diffraction plane of the Ag thin films based on the Scherrer formula [24]:

$$D = \frac{0.91\lambda}{B\cos\theta_B} \quad (1)$$

where θ_B is the Bragg angle of the diffraction lines, λ is the wavelength of the incident X-ray, and B is the full width at half maximum (FWHM) of the diffraction peak. The thicknesses of the ITO or ITO/Ag multi-layers were measured by a surface profiler. Field Emission Scanning electron microscopy (FESEM, Hitachi S- 4800) operated by 15 kV was employed to observe the surface morphology for the ITO layer, AI and IAI multilayer. The microstructures of the stacked samples were observed by transmission electron microscopy (TEM, JEOL JEM -2010, 200 kV). The surface roughness of the ITO stacked films were evaluated using a Digital Instruments atomic force microscope (AFM) with tapping mode over a 2×2 or 5×5 μm^2 scanning area. The X-ray photoelectron spectroscopy (XPS) measurements were carried out at RT. Thermo K-alpha with Al *K*α line (1486.6 eV) as excitation source has been used. The binding energies were calibrated based on the C*1s* peak at 284.5 eV as a reference. Depth profiling with XPS was carried out by using Ar ion sputtering with operation voltage of 3 kV and beam current density of 1 pA/m^2. The optical properties of the ITO, AI, and IAI series samples were characterized by a JASCO V670 UV/VIS/NIR spectrometer. The spectral transmittance (*T*) and reflectance (*R*) were measured at normal incidence at wavelengths (λ) ranging from 300 to 2500 nm. The sheet resistances (*Rs*) of the deposited films were determined using a four-point-probe system with a constant current of 1 mA. The carrier concentration and mobility of the AI, and IAI multilayer were also extracted by a Hall Effect measurement system following the Van der Pauw method.

3. Results and Discussion

3.1 Structure and optical properties of ITO films fabricated by reactive sputtering with different O_2/Ar ratio

The film growth rate of a ITO layer fabricated by reactive sputtering with different O_2/Ar mixture on glass was measured by a surface profiler and confirmed by cross-sectional FESEM. The optical properties of the 60-nm-thick ITO layer on glass grown with different O_2/Ar mixtures at RT were also explored. The UV/visible transmittance of the ITO film with different O_2/Ar mixtures of 0, 1 or 2% are shown in Fig. 1(a). The transmittance of the ITO film at a wavelength of 550 nm exceeded 75 %. The optical band gap (Eg) can be extracted using the absorption coefficient (α) and the relationship between $(\alpha h\nu)^2$ and photon energy ($h\nu$), which considers the direct allowable optical transition of ITO layer. The extracted optical band gap of the RF reactive sputtering-prepared ITO layer with O_2/Ar mixture of 1% for the ITO/glass

configuration was approximately 3.62 eV (Fig. 1(b)), which is consistent with the value presented in the literature for a ITO layer [25]. With a 1% of O_2/Ar mixture during deposition, the visible transmittance within the wavelength ranging from 400 to 700 nm in the ITO film was improved. Some O-vacancies in the ITO layer by introducing appropriate amount O_2 gas may be annihilation, which leaded to this result. The XRD diffraction of the 60-nm-thick ITO film was also carried out to reveal that the crystal structure of 60-nm-thick ITO film was amorphous (not shown here). All of the ITO layers in this work were prepared by RF magnetron reactive sputtering with O_2/Ar gas flow ratio of 1%.

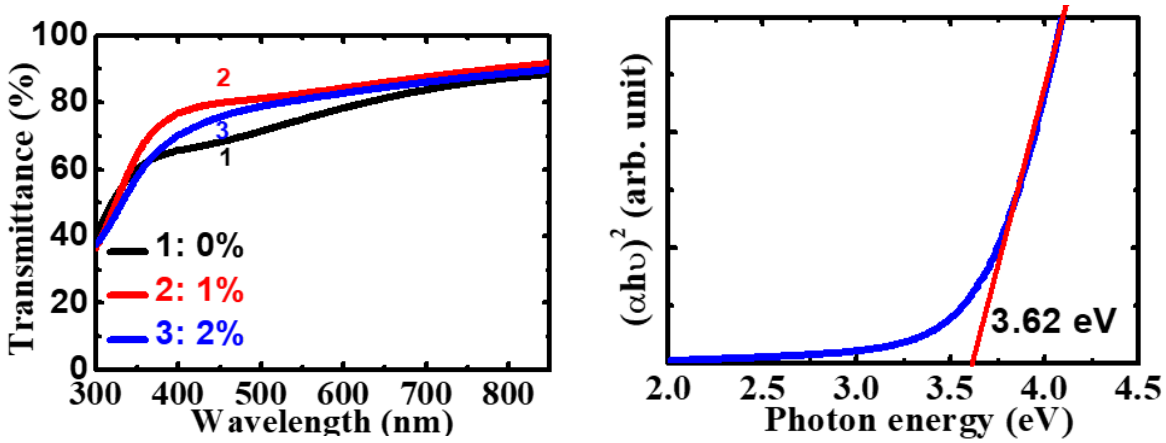

Fig. 1. (a) Optical transmittance of 60-nm-thick ITO/glass as a function of O_2/Ar ratio during deposition, (b) the extracted optical band gap of ITO with a 1% of O_2/Ar ratio.

3.2 Structure, electrical and optical properties of AI stacked layer prepared with Ag under O_2/Ar plasma exposure

After nominal 10-nm-thick Ag deposition on a 60-nm-thick ITO/glass, some AI stacked layers were exposed to O_2/Ar mixture plasma irradiation for different processing time and introducing gas ratio. The AI-0, AI-1, and AI-6 referred the samples to be without any post-deposition plasma treatment, treated with 5 min through a O_2/Ar flow rate ratio of 1% and 6%, respectively. In Fig. 2(a), the transmittance of AI-1 is higher than that of AI-0 within the wavelength range between 300 ~ 1000 nm. At the wavelength of 550 nm, the transmittance in sample AI-1 can increase 15% higher than that of AI-0. In the near infra red region (1000 ~ 2500 nm), the transmittance of AI-1 is almost the same as that of AI-0. The transmittance in the sample AI-6 show different characteristics with AI-0 and AI-6, which the magnitude of the transmittance increases monotonically within the wavelength range, peaks at the wavelength of

1600 nm, then slightly decrease down to 82% at the wavelength of 2500 nm. The GIAXRD were adopted to examine the crystallinity for the three samples as shown in Fig. 2(b). The XRD spectra for the AI-0 and AI-1 samples did not show obvious discrepancy. The peaks around 38.2° and 44.6° are attributed to the Ag (111) orientation and Ag (200) orientations, respectively [JCPDS card number: 04–0783]. The lattice constant of the Ag layer in this work was 0.401 nm, which is nearly the same as the theoretical value (0.409 nm). With an identical Ag thickness (10 nm), the grain size of the (111)-oriented Ag grain measuring 9.8 nm is larger than that of the (200)-oriented Ag grain measuring 4.8 nm. These XRD results suggest that the crystallinity of the two samples were similar. In contrast, the diffraction peaks of Ag(111) and (220) in sample AI-6 disappear and the peaks around the diffraction angle of 31° were broaden, which may be attributed to the formation of AgO_x layer [20, 26].

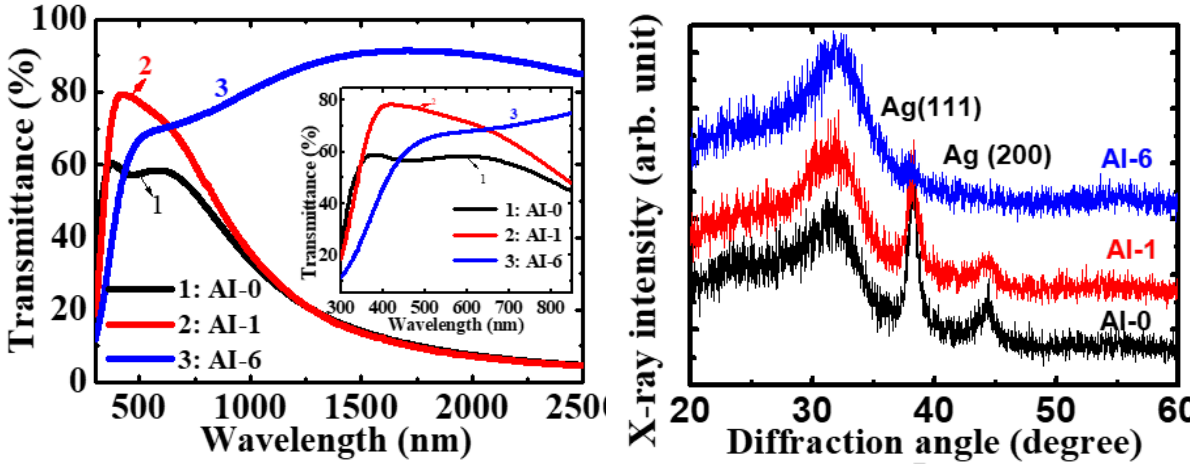

Fig. 2. (a) Optical transmittance and (b) the X-ray patterns for A(10)I(60) with Ag layer under different O_2/Ar ratio exposure. The insert one in (a) is the enlarge plot of the transmittance within the wavelength ranging from 300 to 850 nm.

In Fig. 3, the surface morphology of the AI series samples were revealed by plan-view FESEM. There were still some voids on the surface of sample AI-0, but few voids can be observed on the surface of AI-1 and AI-6. The surface roughness of the AI series samples were also characterized with AFM (Fig. 4). the surface roughness of AI-0, AI-1, and AI-6 are 2.16, 0.74, and 0.78 nm, respectively. This result suggests that surface morphology of AI can be tailored by post-deposition plasma irradiation by introducing O_2/Ar mixtures. High roughness in Ag surface will suppress the transmittance of the visible photons. The AI-1 with smooth surface can be achieved higher visible transmittance as shown in Fig. 2(a). According to the electrical properties obtained by four point probe, the sheet resistance (Rs) for the two samples

were the same (4.8 Ω/sq) as shown in Fig. 5. The O_2/Ar plasma mixtures can modify the surface of Ag nanocluster on ITO buried layer, which achieved a continuous film with a thin thickness and smooth surface. The performance of the ITO and Ag based multilayers as a transparent electrode was also compared using a figure of merit (FOM) [27]. The FOM for all of the as-prepared multilayers was calculated using the formula

$$FOM = \frac{T^{10}}{R_s}, \tag{2}$$

where T is the transmittance at the wavelength of 550 nm and *R*s is the sheet resistance of the AI or multilayer coatings. Owing to thin Ag thickness with an enough electrical path, this characteristic may lead to the AI-1 sample with a high visible FOM at the wavelength of 550 nm.

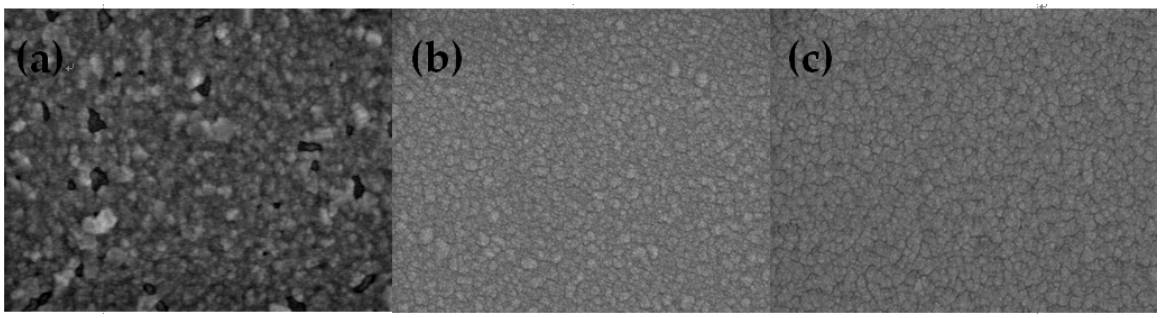

Fig. 3. Top view SEM micrographs of sample (a) AI-0, (b) AI-1, and (c) AI-6.

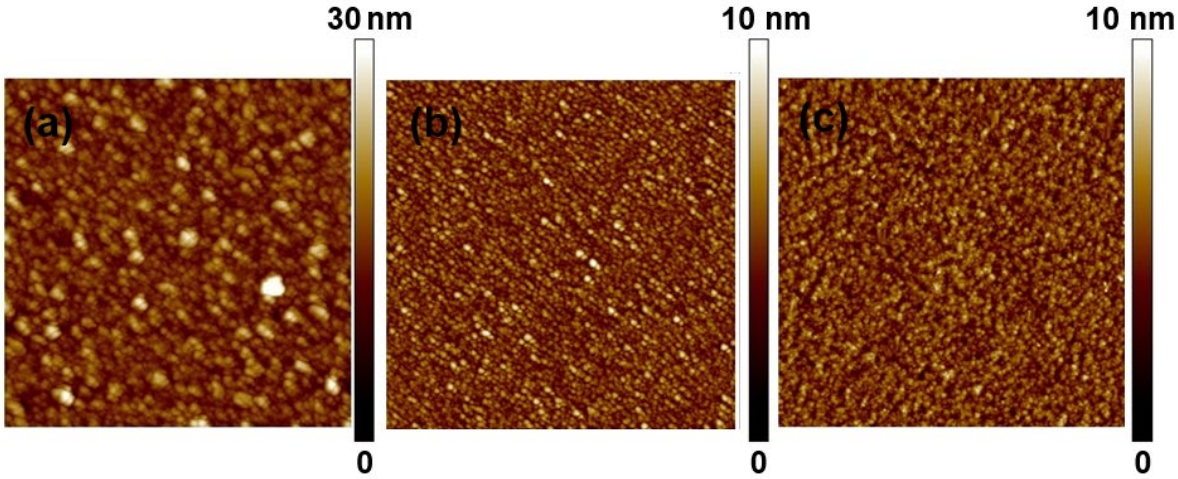

Fig. 4. AFM surface morphology of sample (a) AI-0, (b) AI-1, and (c) AI-6

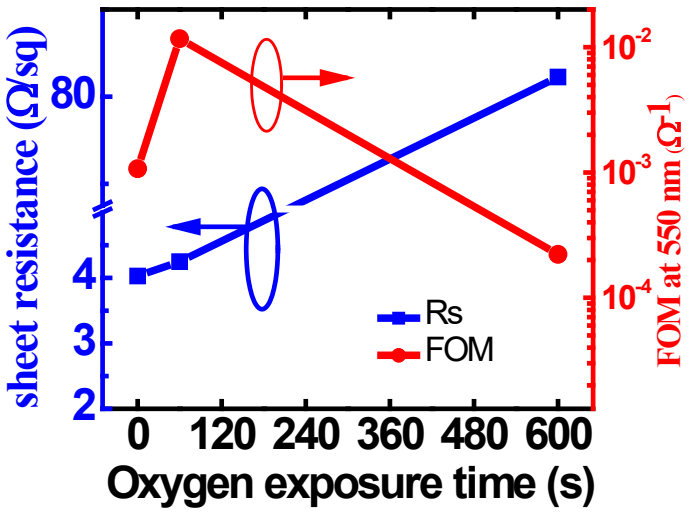

Fig. 5. Sheet resistance and the FOM for the AI series samples.

3.3 Structure, optical, and electrical properties of symmetrical IAI stacked layer with different Ag thickness

Effects of the Ag mid-layer exposed to O_2/Ar plasma for different duration on the visible transmittance of IAI samples were also investigated. The O_2/Ar flow rate ratio was kept at 1%. After exposure of the O_2/Ar mixture plasma (300 s), different thickness in ITO layer were then covered on the prior AI stacked layer. Fig. 6 shows cross-sectional TEM images of the IAI multilayer with a nominal 10-nm-thick Ag layer. The IA(10)I stacked layer clearly revealed well-defined ITO and Ag layers without the formation of an interface layer. There is no obvious evidence of an interfacial reaction between the Ag and ITO layers due to the stability of the coexistence of the ITO and Ag layers at RT, even Ag was exposed under 1% of O_2/Ar flow. Considering the formation enthalpy of In_2O_3 (-923.6 kJ/mol) and SnO_2 (-577.6 kJ/mol), the dissociation of ITO by the formation of a Ag_2O (-31.1 kJ/mol) layer cannot easily occur due to the higher free energy of the formation for the In_2O_3 (-923.6 kJ/mol) and SnO_2 layer compared to that of the Ag_2O layer [28, 29]. The crystal structure of ITO OL and BL are amorphous, as evidenced by the HRTEM image. This result is consistent with the results of the X-ray spectra obtained from the IAI layer (no diffraction peaks related to Ag_2O phase and ITO was observed). The FWHM and the intensity of the X-ray spectrum for the IAI layer seem to become narrower and higher with the increasing thickness of the inserted Ag layer. No ITO or Ag oxide-related phase with a polycrystalline structure was observed form the X-ray pattern of IAI, which indicates that the structures of the ITO OLs and BLs are amorphous, the Ag oxide was absent.

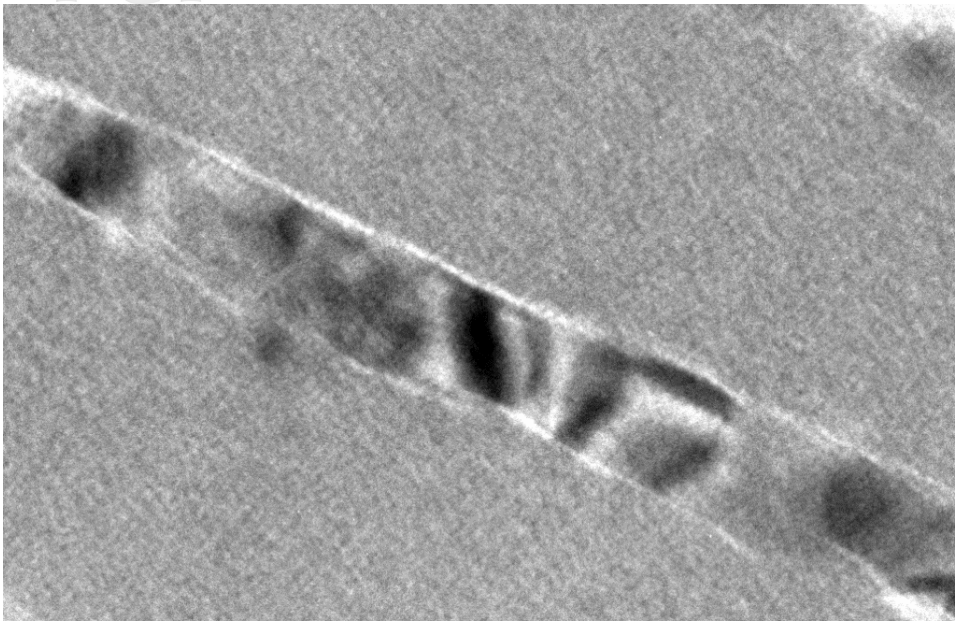

Fig. 6. Cross-sectional high resolution TEM micrograph image of IA(10)I on glass.

In Fig. 7, it presents the XPS depth profile and the core electron signal of Ag obtained from the IAI multilayer with a 10-nm-thick Ag midlayer. The XPS depth profile exhibits well-defined top ITO, Ag and ITO BL. The constant atomic concentration of O, In, and Sn atoms for the top and the bottom ITO layer profile indicated the identical composition. There are no evidence of Ag out-diffusion or oxygen in diffusion into the Ag layer at RT deposition as suggested from the XTEM result. To investigate the interfacial reaction between Ag and ITO layer. The Ag $3d_{5/2}$ and $3d_{3/2}$ peaks in the Fig. 7(b) were revealed an and were shown no-shift of the peak position (368.2 and 374.2 eV) with increasing sputtering depth in the proximity of the ITO top layer and the inserted Ag layer. The invariable peak position of Ag $3d_{5/2}$ and $3d_{3/2}$ signal indicates that there is no interfacial reaction or formation of Ag_2O layer in the proximity of interface region between the ITO and Ag layer.

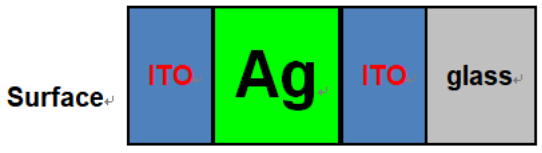

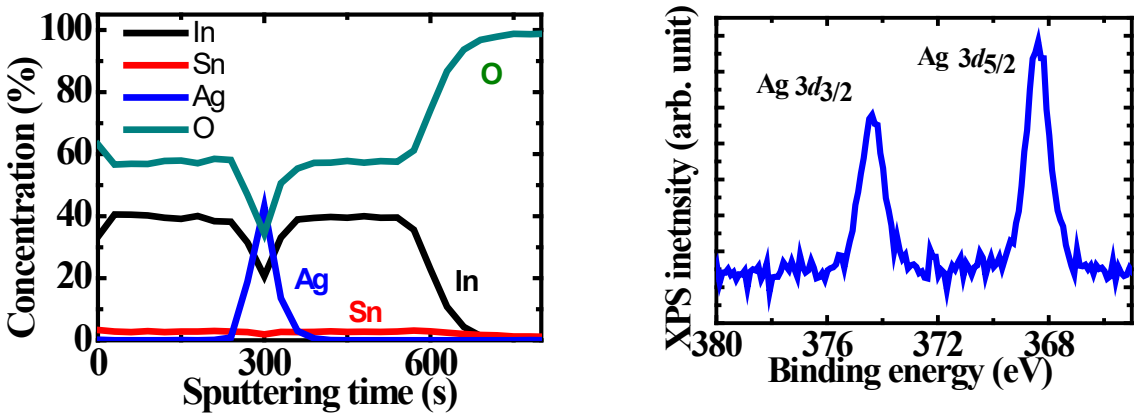

(a) (b)

Fig. 7. (a) Depth profile of the IA(10)I multilayer on glass, (b) the Ag 3d peak obtained from the inserted Ag layer.

The UV-Vis spectra of IAI multi-layers with different Ag-layer thickness and ITO film of 60 nm are shown in Fig. 8(a). In Fig. 8(b), the transmittance at a wavelength of 550 nm for the IAI stacked layers were 87.9, 96.4, 95.6, 92.2, and 90.7 % for Ag layer thicknesses of 6.2, 8.6, 10, 12, and 15 nm, respectively. Meanwhile, the average visible transmittance (T_{ave}) form the wavelength of 400 to 850 nm for the IAI multilayers were 77.2, 90.5, 89.4, 85, and 81.7 % for Ag layer thicknesses of 6.2, 8.6, 10, 12, and 15 nm, respectively. The symmetric IAI stacked layer with a 8.6-nm-thick Ag layer can achieve the highest visible transmittance at the wavelength of 550 nm. The transmittance value of IAI at the wavelength of 550 nm and T_{ave} associated with an increasing Ag thickness show an initial increase followed by a decrease. Owing to discontinuous Ag layer of 6.2 nm, the incident photons within the wavelength between 400 and 850 nm may be scattering, this characteristic lead to the reduction of the transmittance in sample IA(6.2)I. The magnitude of transmittance for sample IA(10)I was comparable to that of IA(8.6)I one. At a sufficiently large thickness (> 10 nm), the Ag mid-layer may create an amplified electric field through metallic surface plasmon resonance [30]. With ITO as the dielectric film, this result may also be responsible for the high visible transmittance of the IAI layer with an 10-nm-thick Ag layer. The IAI stacked layer with an 10-nm-thick Ag layer showed high transparent transmittance (95.6 % at 550 nm). The AI layer with the same Ag-layer thickness also exhibited a lower optical transmittance (550 nm) than that of IAI multilayer (compared with Fig. 2(a)). The ITO capping layer can help to prevent the oxidation of the inserted Ag thin layer and play an important role as an antireflection layer at the visible wavelength.

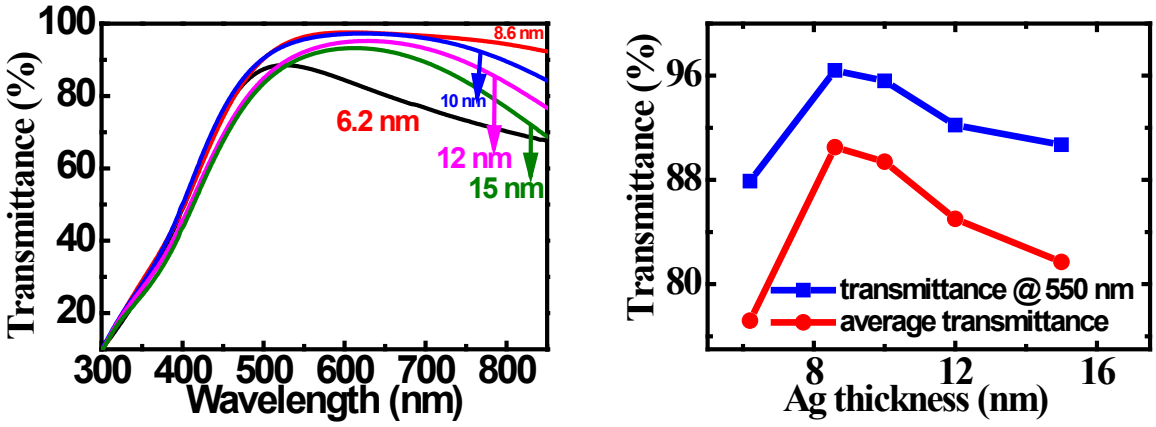

(a) (b)

Figure 8. (a) UV/Visible spectra and (b) the transmittance at the wavelength of 550 nm and the average transmittance from 400 to 850 nm for the IA(n)I multilayers on glass.

The dependence of the *R*s of the IAI multilayers on the inserted Ag thickness is illustrated in Fig. 9(a). The resistance of the as-prepared ITO film was about 82 Ω/sq. The *R*s of the IAI stacked layers were 43.1, 9, 5.8, 4.70, and 4.2 Ω/sq for Ag layer thicknesses of 6.2, 8.6, 10, 12, and 15 nm, respectively. The *R*s of the IAI multilayers was effectively reduced by increasing the thickness of the inserted Ag film. In Fig. 9(b), the carrier concentration and mobility of the IAI multilayered films are presented. For the IAI films, the electron concentrations were 1.01×10^{21}, 5.8×10^{21}, 8.7×10^{21}, 1.04×10^{22}, and 1.34×10^{22} cm^{-3} for Ag layer thickness of 6.2, 8.6, 10, 12, and 15 nm, respectively. The carrier mobility in the IAI layers were in the range between 11.1 and 14.3 $cm^2/V\cdot s$.

In Fig. 9(a), the dependence of the FOM at the wavelength of 550 or 600 nm for the IAI layers on the inserted Ag thickness were also illustrated. The IA(10)I with an *Rs* of 5.8 Ω/sq shows the highest FOM of 1.09×10^{-1} Ω^{-1} at the wavelength of 550 nm and the highest of 1.28×10^{-1} Ω^{-1} at the wavelength of 600 nm. The FOM value of the IA(10)I electrode in this work is higher than previously reported values for ITO and Ag based multilayer [10, 19, 31-32]. The surface morphology of I(60)A(10)I(60) stacked layer was revealed by AFM as shown in Fig. 10. The roughness of the sample was 0.68 nm, which was comparable to that of sample AI-1 (0.76 nm).

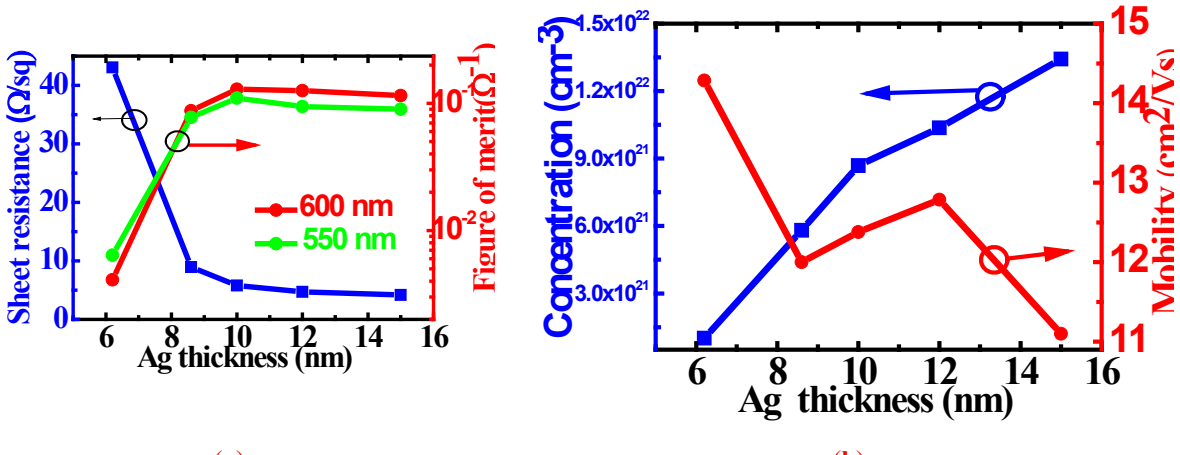

Figure 9. (a) Sheet resistance and FOM at the wavelength of 550 or 600 nm, (b) carrier concentration and mobility for the IA(n)I series samples, the thickness of ITO is 60 nm

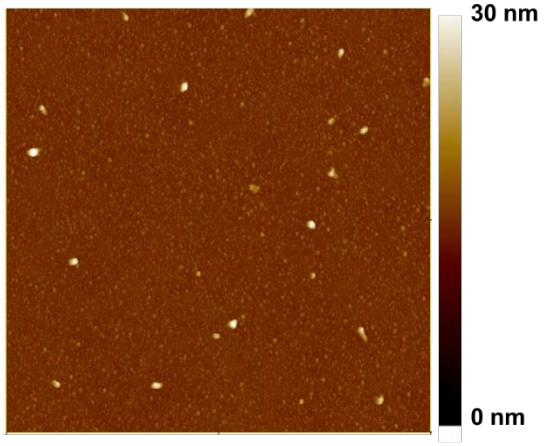

Figure 10. AFM morphology of as-prepared sample IA(10)I.

The transmittance spectra for the symmetric IA(10)I multilayers with different top and bottom ITO thicknesses of 41, 48 and 60 nm are shown in Fig. 11(a). In Fig. 11(b), the position of maximum transmittance in IAI stacked layer depends on its ITO thickness and exhibits a blue-shift. The *R*s and visible transmittance at a wavelength of 550 nm and the FOM of symmetric IAI multilayers with different ITO thickness are listed in Table I. The X-ray spectra of IAI multilayers with different ITO thickness are also carried out to evaluate the crystallinity of Ag midlayer. The FWHM of the Ag (111) peak suggests an improvement in the crystallinity of the Ag layer with the increase in the ITO BLs thickness. The grain size in the Ag layer increases with increasing thickness of the ITO BLs. This relationship is responsible for the lowest *R*s in the I(60)AI(60) stacked layer. A ITO BLs with a sufficiently large thickness can improve the crystallinity of the above inserted Ag layer in IAI structure. The *Rs* of the IAI stacked layer shows a decrease with the increase in the thickness of the ITO. The improvement in Ag crystallinity may be responsible for this result. The magnitude of transmittance in

I(n)AI(n) at the wavelength of 550 nm decreases with an increasing ITO thickness, but the FOM of IAI seem to be a different trend with its ITO thickness. I(60)AI(60) can also achieve a high FOM of 1.09×10^{-2} Ω^{-1} at a wavelength of 550 nm among the symmetrical IAI tri-layer in this work. This characteristic is consistent with that reported for an $TiO_x/Ag/TiO_x$ with different BL configuration [14].

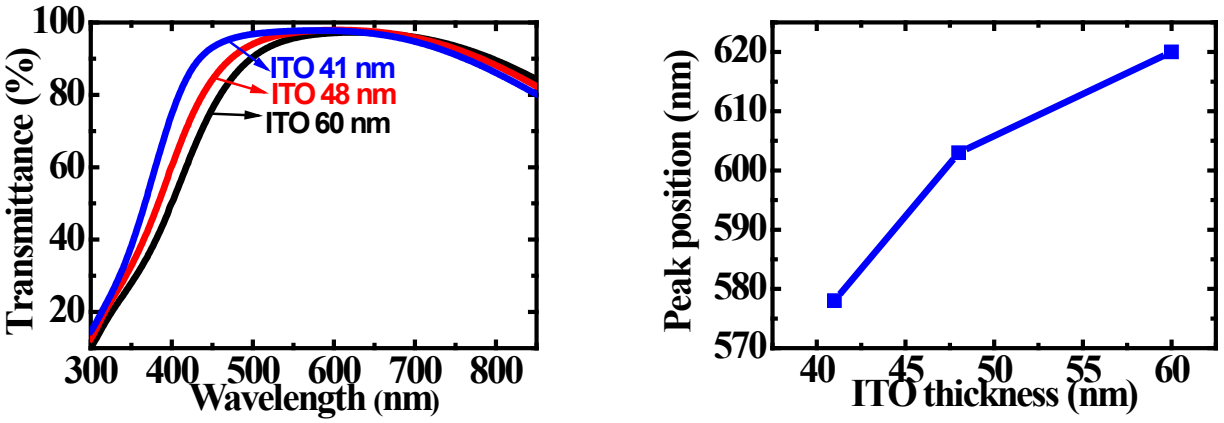

Fig .11. (a) Visible transmittance and (b) the peak position of transmittance of the symmetrical IA(10)I samples with different ITO thickness.

Table 1. Optical and electrical properties of symmetric IAI stacked layer films with different ITO BL or IL thickness

Thickness (nm)	Transmittance at 550 nm (%)	Sheet resistance (Ω/sq)	FOM (Ω^{-1})
41/10/41	97.7	6.45	0.122
48/10/48	97.2	6.27	0.119
60/10/60	95.6	5.80	0.109

4. Conclusions

The crystallinity, microstructure, and electrical, optical properties and thermal stability of ITO and ITO/Ag multi-layers on soda-lime glass were studied. The ITO layers with amorphous phases fabricated by reactive sputtering with plasma through O2/Ar mixture of 1% severed as the reactive gas exhibited high visible transmittance and a large optical band gap of 3.62 eV.

The Ag layer was exposed to plasma irradiation induced by in-situ 1% O2/Ar mixture, this approach was demonstrated to reduced the surface roughness and tune the visible transmittance of AI effectively without degradation of Ag crystallinity and Rs of AI. In the IAI multilayer, the interface between the Ag and ITO layer revealed by HRTEM shows a distinct boundary. With an embedded Ag layer > 10 nm, the as-prepared IAI sandwiched layers exhibit superior conductivity with high visible transmittance at the wavelength of 550 and 600 nm. The inserted 10-nm Ag layer can effectively reduce the resistance of the I(60)A(10)I(60) stacked layer down to 5.8 Ω/sq, and the FOM of IA(10)I at a visible wavelength of 550 and 600 nm can reach up to ~ 1.09×10-1 and 1.28×10-1 Ω-1. The visible transmittance of symmetric IAI sample shows a blue-shift with a decreasing in the ITO thicknesses. Our results suggest that a ITO multilayer with appropriate Ag and ITO thicknesses is a promising electrode candidate for application as a TCO.

References

[1] Hecht, D. S.; Hu, L. B.; Irvin, G., Emerging Transparent Electrodes Based on Thin Films of Carbon Nanotubes, Graphene, and Metallic Nanostructures. *Adv. Mater.* **2011,** *23* (13), 1482-1513.

[2] Granqvist, C. G., Transparent conductors as solar energy materials: A panoramic review. *Sol. Energy Mater. Sol. Cells* **2007,** *91* (17), 1529-1598.

[3] Lim, S. H.; Kim, H. K., Deposition Rate Effect on Optical and Electrical Properties of Thermally Evaporated WO_{3-x}/Ag/WO_{3-x} Multilayer Electrode for Transparent and Flexible Thin Film Heaters. *Sci Rep* **2020,** *10* : 8357.

[4] Goncalves, G.; Elangovan, E.; Barquinha, P.; Pereira, L.; Martins, R.; Fortunato, E., Influence of post-annealing temperature on the properties exhibited by ITO, IZO and GZO thin films. *Thin Solid Films* **2007,** *515* (24), 8562-8566.

[5] Chen, S. W.; Koo, C. H., ITO-Ag alloy-ITO film with stable and high conductivity depending on the control of atomically flat interface. *Mater. Lett.* **2007,** *61* (19-20), 4097-4099.

[6] Zhang, Z. B.; Zhang, X. Y.; Xu, L. G.; Yang, Y. N.; Min, P. P.; Zhang, R. C.;

Yang, L.; Bolshakov, A.; Zhu, J. Q., Improved stability of dielectric/metal/dielectric-structured transparent conductive films with the insertion of Ni layer under thermal oxidation environment. *Mater. Lett.* **2021,** *282*, 128844.

[7] Cattin, L.; El Mahlali, A.; Cherif, M. A.; Touihri, S.; El Jouad, Z.; Mouchaal, Y.; Blanchard, P.; Louarn, G.; Essaidi, H.; Addou, M.; Khelil, A.; Torchio, P.; Bernede, J. C., New dielectric/metal/dielectric electrode for organic photovoltaic cells using Cu:Al alloy as metal. *J. Alloy. Compd.* **2020,** *819*, 8.152974

[8] Kim, S.; Lee, J. L., Design of dielectric/metal/dielectric transparent electrodes for flexible electronics. *J. Photonics Energy* **2012,** 2(2), 021215.

[9] Sivaramakrishnan, K.; Alford, T. L., Conduction and transmission analysis in gold nanolayers embedded in zinc oxide for flexible electronics. *Appl. Phys. Lett.* **2010,** *96* (20), 201109.

[10] Rwenyagila, E. R.; Agyei-Tuffour, B.; Kana, M. G. Z.; Akin-Ojo, O.; Soboyejo,. W. O., Optical properties of ZnO/Al/ZnO multilayer films for large area transparent electrodes. J. Mater. Res. 2014, **29**, 2912-2920.

[11] Dhar, A.; Alford, T. L., Optimization of TiO_2/Cu/TiO**2** Multilayer as Transparent Composite Electrode (TCE) Deposited on Flexible Substrate at Room Temperature. *ECS Solid State Lett.* **2014,** *3* (11), N33-N36.

[12] Cheng, C. H.; Ting, J. M., Transparent conducting GZO, Pt/GZO, and GZO/Pt/GZO thin films. *Thin Solid Films* **2007,** *516* (2-4), 203-207.

[13] Kumar, M. M. D.; Baek, S. M.; Kim, J., The influence of Ni layer and thickness of AZO layers on the optoelectronic properties of AZO/Ni/AZO tri-layer deposited at room temperature. *Mater. Lett.* **2014,** *137*, 132-135.

[14] Peng, C. H.; Chen, P. S.; Lo, J. W.; Lin, T. W.; Lee, S. W., Indium-free transparent TiOx/Ag/WO3 stacked composite electrode with improved moisture resistance. *J. Mater. Sci.*-

Mater. Electron. **2016,** *27* (11), 12060-12066.

[15] Liu, X. N.; Gao, J.; Gong, J. H.; Wang, W. X.; Chen, S. C.; Dai, M. J.; Lin, S. S.; Shi, Q.; Sun, H., Optoelectronic properties of an AZO/Ag multilayer employed as a flexible electrode. *Ceram. Int.* **2021,** *47* (4), 5671-5676.

[16] Fan J. C. C.; Bachner F. J.; Foley G. H.; Zavracky P. M., Transparent heat-mirror films of TiO2/Ag/TiO2 for solar energy collection and radiation insulation. Appl. Phys. Lett. 1974, 25, 693-695.

[17] Park, Y. S.; Choi, K. H.; Kim, H. K., Room temperature flexible and transparent ITO/Ag/ITO electrode grown on flexile PES substrate by continuous roll-to-roll sputtering for flexible organic photovoltaics. *J. Phys. D-Appl. Phys.* **2009,** *42* (23), 235109.

[18] Park, S.; Yoon, J.; Kim, S.; Song, P., Hydrogen-driven dramatically improved mechanical properties of amorphized ITO-Ag-ITO thin films. *RSC Adv.* **2021,** *11* (6), 3439-3444.

[19] Ren, N. Y.; Zhu, J.; Ban, S. L., Highly transparent conductive ITO/Ag/ITO trilayer films deposited by RF sputtering at room temperature. *AIP Adv.* **2017,** *7* (5), 055009.

[20] Wang, W.; Bae, T. S.; Park, Y. H.; Kim, D. H.; Lee, S.; Min, G. H.; Lee, G. H.; Song, M.; Yun, J., Highly efficient and bendable organic solar cells using a three-dimensional transparent conducting electrode. *Nanoscale* **2014,** *6* (12), 6911-6924.

[21] Han, Y. C.; Lim, M. S.; Park, J. H.; Choi, K. C., Optical Effect of Surface Morphology of Ag on Multilayer Electrode Applications for OLEDs. *IEEE Electron Device Lett.* **2014,** *35* (2), 238-240.

[22] Cattin, L.; Lare, Y.; Makha, M.; Fleury, M.; Chandezon, F.; Abachi, T.; Morsli, M.; Napo, K.; Addou, M.; Bernede, J. C., Effect of the Ag deposition rate on the properties of conductive transparent MoO3/Ag/MoO3 multilayers. *Sol. Energy Mater. Sol. Cells* **2013,** *117*, 103-109.

[23] Antad, V.; Simonot, L.; Babonneau, D., Tuning the surface plasmon resonance of silver nanoclusters by oxygen exposure and low-energy plasma annealing. *Nanotechnology* **2013,** *24* (4), 045606.

[24] Cullity B. D.; Stock S. R., in Elements of X-ray Diffraction, chap. 3, p. 170, Prentice-Hall, Englewood Cliffs, NJ (2001).

[25] Tuna, O.; Selamet, Y.; Aygun, G.; Ozyuzer, L., High quality ITO thin films grown by dc and RF sputtering without oxygen. *J. Phys. D-Appl. Phys.* **2010,** *43* (5), **43**, 055402.

[26] Pierson, J. F.; Rousselot, C., Stability of reactively sputtered silver oxide films. *Surf. Coat. Technol.* **2005,** *200* (1-4), 276-279.

[27] Haacke G., New figure of merit for transparent conductors, J. Appl. Phys. **1976**, **47** 4086-4089.

[28] Lide D. R., CRC Handbook of Chemistry and Physics, 76th ed. (CRC, Boca Raton, FL, 1995).

[29] Jeong, J. A.; Kim, H. K., Low resistance and highly transparent ITO-Ag-ITO multilayer electrode using surface plasmon resonance of Ag layer for bulk-heterojunction organic solar cells. *Sol. Energy Mater. Sol. Cells* **2009,** *93* (10), 1801-1809.

[30] Zhang, D. Y.; Wang, P. P.; Murakami, R.; Song, X. P., Effect of an interface charge density wave on surface plasmon resonance in ZnO/Ag/ZnO thin films. *Appl. Phys. Lett.* **2010,** *96* (23) 233114.

[31] Guillen, C.; Herrero, J., Transparent conductive ITO/Ag/ITO multilayer electrodes deposited by sputtering at room temperature. *Opt. Commun.* **2009,** *282* (4), 574-578.

[32] Indluru, A.; Alford, T. L., Effect of Ag thickness on electrical transport and optical properties of indium tin oxide-Ag-indium tin oxide multilayers. *J. Appl. Phys.* **2009,** *105* (12), 123528.